CHAOS
Theory and Applications
in Applied Sciences and Engineering

e-ISSN: 2687-4539
RESEARCH ARTICLE
Vol.6 / No.3 / 2024 / pp.192-204
https://doi.org/10.51537/chaos.1300754

Chaotic Dynamics of the Fractional Order Predator-Prey Model Incorporating Gompertz Growth on Prey with Ivlev Functional Response

Md. Jasim Uddin *,1, **P. K. Santra** α,2, **Sarker Md. Sohel Rana** *,3 and **G. S. Mahapatra** §,4

*Department of Mathematics, University of Dhaka, Dhaka-1000, Bangladesh, αAbada Nsup School, Abada, Sankrail-711313, Howrah, India, §Department of Mathematics, National Institute of Technology Puducherry, Karaikal-609609, India.

ABSTRACT This paper examines dynamic behaviours of a two-species discrete fractional order predator-prey system with functional response form of Ivlev along with Gompertz growth of prey population. A discretization scheme is first applied to get Caputo fractional differential system for the prey-predator model. This study identifies certain conditions for the local asymptotic stability at the fixed points of the proposed prey-predator model. The existence and direction of the period-doubling bifurcation, Neimark-Sacker bifurcation, and Control Chaos are examined for the discrete-time domain. As the bifurcation parameter increases, the system displays chaotic behaviour. For various model parameters, bifurcation diagrams, phase portraits, and time graphs are obtained. Theoretical predictions and long-term chaotic behaviour are supported by numerical simulations across a wide variety of parameters. This article aims to offer an OGY and state feedback strategy that can stabilize chaotic orbits at a precarious equilibrium point.

KEYWORDS
Prey-predator model
Fractional order
Bifurcations
Maximum Lyapunov Exponents
Fractal dimensions
Chaos control

INTRODUCTION

In the ecology, predation and prey behaviors are frequent occurrences. Since Volterra and Lotka developed the predator-prey paradigm in the 20th century, several academics have expressed worry about it. Numerous researchers have made significant adjustments to the system by including ecological elements such functional responses, emigration and immigration (Kangalgil and Işık 2022), time delays (Li *et al.* 2022b), diffusion (Sun *et al.* 2022), and the Allee effect (Zhao and Du 2016) because this system has disregarded many real-world scenarios. The study of the intricate dynamical behaviors of predator-prey systems has recently attracted growing interest (Atabaigi 2020; Din 2017; Işık 2019; Kartal 2014, 2017). In any prey-predator encounter, the functional response in population dynamics is a key component as it refers to the quantity of prey consumed by a predator based on the density of the prey in per unit of time. The Holling type II Holling (1965) is suitable for the majority of arthropod predators as the functional response compare to others form Holling type I, III, IV. In the first quadratic, these functional responses are uniformly bounded functions in addition to being monotonically increasing. Ivlev Ivlev (1961) proposed a different functional response, known as the Ivlev functional response, to study the dynamical interaction between prey and predator species: $p(x) = b(1 - e^{-ax})y$, where the maximal rate of predation and the decline in hunting drive are represented by the positive constants b and a, respectively.

Numerous studies have been done to examine the predator-prey relationship with Ivlev-type functional responses. The findings suggested that Ivlev-type relation between the species have several systems in ecological applications, including dynamics in predator-prey systems (Cheng *et al.* 1982; Guo *et al.* 2013; Kooij and Zegeling 1996; Wang *et al.* 2010), host-parasite systems (Preedy *et al.* 2007), and animal coat patterns (Uriu and Iwasa 2007). The authors investigated the presence and uniqueness of limit cycles as well as the numerical calculation of phase portraits in these empirical studies. In a predator-prey system (Wei *et al.* 2023), this work examines the dynamical balance and Markov-switching-induced stochastic P-bifurcation.A theoretical foundation for comprehending the spatiotemporal evolution characteristics of plant systems is provided by the findings presented in (Li *et al.* 2022b; Sun *et al.* 2022).

Manuscript received: 22 May 2023,
Revised: 25 February 2024,
Accepted: 5 April 2024.

[1]jasimu00@gmail.com
[2]prasunsantra5@gmail.com (**Corresponding author**)
[3]srana.mthdu@gmail.com
[4]gs.mahapatra@nitpy.ac.in

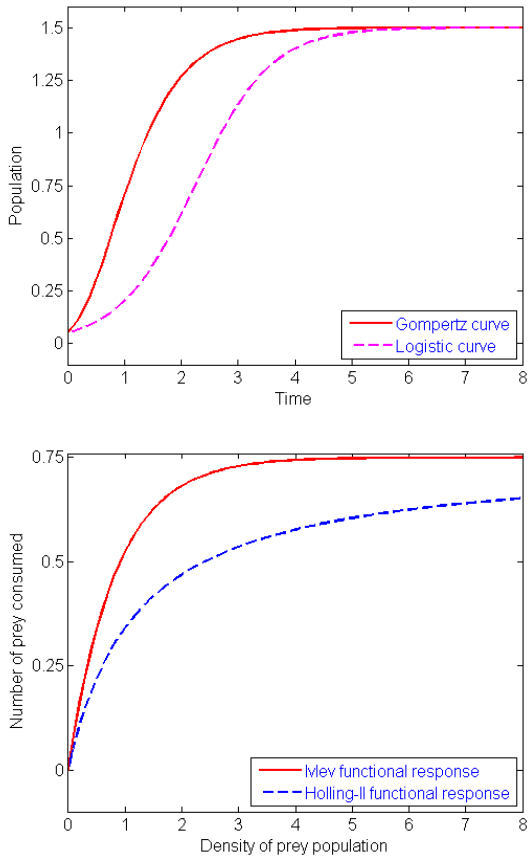

Figure 1 (a) Growth curves (b) Functional responses for $r = 1.5, k = 1.5, a = 1.2, d = 0.4$

When a third party distracts their predators, prey can lessen the burden of exploitation, such type prey-predator model is discussed in (Revilla and Křivan 2022). On the basis of the generalized Klausmeier-Gray-Scott model, authors Li *et al.* (2022a) build an extended vegetation-water model with infiltration delay and discuss dynamic behavior of this model. The long-term coevolution of the giving-up rates of the model of reckless prey and patient predator is studied by Cecilia B. et al. in (Berardo and Geritz 2021) using adaptive dynamics. The majority of predator-prey systems with various functional responses take into account the logistic growth of the prey, according to academics.

Gompertz (1825) created a different prey birth rate interpretation similar to logistic growth to study the dynamics of a community made up of populations of several interacting species. The comparison of functional responses and growth curves are shown in Figure 1. The Gompertz curve expands more rapidly than the logistic curve, we discover. Moreover, the point of inflection for the Gompertz curve occurs earlier than for the logistic curve, and thus reaches carrying capacity a little bit early. Also, compared to the Holling type II functional response, the predation rate reaches its peak significantly earlier in the Ivlev-type functional response. In terms of biology, this suggests that the predation rate is proportionate to the prey population while the prey population is low and saturates to a constant 1 when the prey population is high.

The concept of Gompertz growth on prey will be taken into consideration with accounting of Ivlev functional response for the formulation of the following predator-prey system (Rosenzweig 1971):

$$\begin{aligned} \dot{x} &= rx \ln \frac{k}{x} - (1 - e^{-ax})y, \\ \dot{y} &= (1 - e^{-ax})y - dy. \end{aligned} \tag{1}$$

Here, prey and predator population densities are represented by the time-dependent variables $x(t)$ and $y(t)$, respectively. The carrying capacity is described by the parameter k. The value r represents the growth rate of the prey and the death rate of the predator is represented by the constant d. In this prey-predator model, it is presumed that all variables and parameters are non-negative real numbers.

Fractional calculus is the additional idea used in the creation of our model. Fractional-order differential equations (FD) (Kilbas *et al.* 1993; Connolly 2004; Dzieliński *et al.* 2010) are the most widely used because of their similarities to memory-based systems, which are present in most biological systems (Elsadany and Matouk 2015). In many disciplines, including science, engineering, finance, economics, and epidemiology (Huang *et al.* 2017a, 2018, 2017b; M. *et al.* 2011), fractional-order differential equations can be successfully explained. The description of phenomena that integer order differential equations (IDEs) can't fully simulate can be done using fractional differential equations (Ichise *et al.* 1971).

A nonlinear fractional differential system exhibits the complicated dynamics like a nonlinear differential system does in bifurcation and chaos analysis. It is fascinating to study chaos in fractional-order dynamical systems (Elsadany and Matouk 2015; Abdelaziz *et al.* 2018; Ahmad and Sprott 2003). There are various methods for applying the differentiation notion to arbitrary order. The frequently employed definitions are those proposed by Caputo, Riemann-Liouville, and Grünwald-Letnikov (Podlubny 1999). Academics are interested in a variety of discrete models and demonstrating dynamics of those systems through various bifurcations and chaotic attractors (Khan *et al.* 2022; Rana and Kulsum 2017; Rana 2019). Mathematical quantification of these events is possible.

In this work, we employ the Caputo fractional derivatives on the continuous system (1) to theoretically explain the bifurcation occurrences. Fractional derivatives are defined in many ways. Among the most well-known definitions of fractional derivatives is Caputo's (Čermák *et al.* 2015; Abdeljawad 2011), which is widely applied in practical contexts.

Consider

$$D^{\alpha} g(t) = K^{l-\alpha} g^{(l)}(t), \quad \alpha > 0$$

where g^{l} denotes the $l-$order derivative of $g(t)$, $l = [\alpha]$ is the rounded nearest integer value of α, and K^{q} is the $q-$ order operator for the Riemann-Liouville integral.

$$K^{q} f(t) = \frac{\int_0^t (t - \tau_e)^{q-1} f(\tau_e) d\tau_e}{\Gamma(q)}, \quad q > 0$$

where $\Gamma(.)$ is the Euler gamma function. The "α–order Caputo differential operator is expressed by D^{α}.

The following is the model (1)'s fractional order form

$$\begin{aligned} D^{\alpha} x(t) &= rx(t) \ln \frac{k}{x(t)} - (1 - e^{-ax(t)})y(t) \\ D^{\alpha} y(t) &= (1 - e^{-ax(t)})y(t) - dy(t) \end{aligned} \tag{2}$$

There are many methods for converting the model (1) into discrete form. The piecewise constant approximation (PCA) (Uddin *et al.* 2023) is one among them. The model is discretized using PCA method. Here are the steps:

Assume that model (2) initial conditions are $x(0) = x_0, y(0) = y_0$. The discretized version of model (2) is given as:

$$D^\alpha x(t) = rx([\frac{t}{\rho}]) \ln \frac{k}{x([\frac{t}{\rho}])} - (1 - e^{-ax([\frac{t}{\rho}])})y([\frac{t}{\rho}])$$
$$D^\alpha y(t) = (1 - e^{-ax([\frac{t}{\rho}])})y([\frac{t}{\rho}]) - dy([\frac{t}{\rho}])$$

Initially consider $t \in [0, \rho)$, so $\frac{t}{\rho} \in [0, 1)$. Then, we get

$$\begin{aligned} D^\alpha x(t) &= rx_0 \ln \frac{k}{x_0} - (1 - e^{-ax_0})y_0 \\ D^\alpha y(t) &= (1 - e^{-ax_0})y_0 - dy_0 \end{aligned} \tag{3}$$

The solution of (3) can be written as

$$\begin{aligned} x_1(t) &= x_0 + J^\alpha \left(rx_0 \ln \frac{k}{x_0} - (1 - e^{-ax_0})y_0 \right) \\ &= x_0 + \frac{t^\alpha}{\alpha\Gamma(\alpha)} \left(rx_0 \ln \frac{k}{x_0} - (1 - e^{-ax_0})y_0 \right), \\ y_1(t) &= y_0 + J^\alpha \left((1 - e^{-ax_0})y_0 - dy_0 \right) \\ &= y_0 + \frac{t^\alpha}{\alpha\Gamma(\alpha)} \left((1 - e^{-ax_0})y_0 - dy_0 \right). \end{aligned}$$

Then consider $t \in [\rho, 2\rho)$, so $\frac{t}{\rho} \in [1, 2)$. Then

$$\begin{aligned} D^\alpha x(t) &= rx_1 \ln \frac{k}{x_1} - (1 - e^{-ax_1})y_1 \\ D^\alpha y(t) &= (1 - e^{-ax_1})y_1 - dy_1 \end{aligned} \tag{4}$$

which have the following solution

$$\begin{aligned} x_2(t) &= x_1(\rho) + J^\alpha_\rho \left(rx_1 \ln \frac{k}{x_1} - (1 - e^{-ax_1})y_1 \right) \\ &= x_1(\rho) + \frac{(t-\rho)^\alpha}{\alpha\Gamma(\alpha)} \left(rx_1 \ln \frac{k}{x_1} - (1 - e^{-ax_1})y_1 \right), \\ y_2(t) &= y_1(\rho) + J^\alpha_\rho \left((1 - e^{-ax_1})y_1 - dy_1 \right) \\ &= y_1(\rho) + \frac{(t-\rho)^\alpha}{\alpha\Gamma(\alpha)} \left((1 - e^{-ax_1})y_1 - dy_1 \right), \end{aligned} \tag{5}$$

where $J^\alpha_\rho \equiv \frac{1}{\Gamma(\alpha)} \int_\rho^t (t - \tau_e)^{\alpha-1} d\tau_e, \quad \alpha > 0$. After repeating n times, we get

$$\begin{aligned} x_{n+1}(t) &= x_n(n\rho) + \frac{(t-n\rho)^\alpha}{\alpha\Gamma(\alpha)} \left(rx_n(n\rho) \ln \frac{k}{x_n(n\rho)} \right. \\ &\left. -(1 - e^{-ax_n(n\rho)})y_n(n\rho) \right), \\ y_{n+1}(t) &= y_n(n\rho) + \frac{(t-n\rho)^\alpha}{\alpha\Gamma(\alpha)} \left((1 - e^{-ax_n(n\rho)})y_n(n\rho) - dy_n(n\rho) \right), \end{aligned} \tag{6}$$

where $t \in [n\rho, (n+1)\rho)$. For $t \longrightarrow (n+1)\rho$, model (6) becomes

$$\begin{aligned} x_{n+1} &= x_n + \frac{\rho^\alpha}{\Gamma(\alpha+1)} \left(rx_n \ln \frac{k}{x_n} - (1 - e^{-ax_n})y_n \right), \\ y_{n+1} &= y_n + \frac{\rho^\alpha}{\Gamma(\alpha+1)} \left((1 - e^{-ax_n})y_n - dy_n \right). \end{aligned} \tag{7}$$

In this context, ρ represents the step size, while α represents the fractional order. Both parameter values are selected from the interval $(0, 1]$. The remaining parameters have the same range and meaning as defined in equation (1). The Fractional Order Predator-Prey Model incorporating Gompertz growth on prey with Ivlev functional response is a mathematical model designed to capture the dynamics of predator-prey interactions in a more nuanced and realistic way. Let's break down the components and motivations behind this model:

Fractional Order Dynamics: Traditional predator-prey models often use ordinary differential equations (ODEs) with integer-order derivatives. However, fractional calculus allows for the consideration of non-integer order derivatives, offering a more flexible and accurate representation of complex systems. Fractional order models are particularly useful in capturing long-term memory effects and non-local interactions, making them suitable for describing ecological systems with delayed responses.

Gompertz Growth on Prey: The Gompertz growth model is commonly used to describe the growth of biological populations, where the growth rate decreases exponentially over time. Incorporating Gompertz growth in the prey population allows the model to account for the realistic limitation on prey population growth as it reaches carrying capacity. This is especially relevant in ecological systems where resources are finite.

Ivlev Functional Response: Motivation: The functional response describes how the feeding rate of predators changes with the abundance of prey. The Ivlev functional response is one of the many functional response forms, and it considers the saturation of a predator's feeding rate as prey abundance increases. This is crucial for capturing realistic predator-prey interactions, where a predator's feeding rate is not constant but saturates as prey becomes more abundant.

Integration of Components: Motivation: By combining fractional order dynamics, Gompertz growth on prey, and the Ivlev functional response, the model aims to provide a more comprehensive representation of the complex and dynamic nature of predator-prey interactions. This integration allows for a more realistic portrayal of ecological systems by accounting for memory effects, finite resources, and the nonlinear nature of predation.

In summary, the motivation behind the Fractional Order Predator-Prey Model incorporating Gompertz growth on prey with Ivlev functional response lies in the desire to create a more accurate and nuanced mathematical representation of ecological systems. By considering fractional order dynamics, realistic prey growth dynamics, and a biologically relevant functional response, the model aims to improve our understanding of the intricate interplay between predators and prey in natural ecosystems.

While there may not be specific studies or examples explicitly using the exact combination of a Fractional Order Predator-Prey Model with Gompertz growth on prey and Ivlev functional response, you can envision scenarios where such a model might find application. Here are two hypothetical examples:

Fisheries Management: Consider a marine ecosystem where a specific fish species (predator) preys on a population of smaller fish (prey). The fractional order dynamics help account for historical fishing pressures and the impact of environmental changes on the predator-prey relationship. The Gompertz growth model is applied to the prey population, considering resource limitations and environmental factors. The Ivlev functional response reflects the saturation of the predator's feeding rate as the prey becomes more abundant.

Fisheries managers could use this model to predict the effects of fishing quotas, environmental changes, or other interventions on the stability and sustainability of the fishery. It provides a more nuanced understanding of the dynamics involved, aiding in the development of effective management strategies.

Agricultural Pest Control: In an agricultural setting, consider a scenario where a certain insect species (prey) is damaging crops, and a predator species (such as a bird or insect) is introduced for pest control. The fractional order dynamics capture the long-term impact of past pest control measures on predator-prey interactions. The Gompertz growth model represents the natural growth constraints of the pest population due to resource limitations. The Ivlev functional response reflects the saturation in the predator's consumption rate as the pest population increases.

Farmers and pest control agencies could use this model to optimize the introduction of natural predators for pest management. By understanding how past interventions, environmental factors, and prey-predator interactions interact, they can implement more targeted and sustainable pest control strategies.

These examples illustrate how the combination of fractional order dynamics, Gompertz growth on prey, and Ivlev functional response could be applied in different ecological and management contexts to gain insights and inform decision-making.

The remaining sections are arranged as follows. The presence and stability of fixed points are discussed in Section 2. The conditions for codimension-one bifurcations are established such as Neimark-Sacker and period-doubling bifurcations in Section 3. Section 4 presents the prerequisites for Marottos chaos to exist. The results of numerical simulations are presented in Section 5 to demonstrate new and rich dynamic behavior to validate the theoretical analysis. In Section 6, we employ the OGY (Edward *et al.* (1990)) and state feedback control strategies to reduce the chaos of the unmanaged system. Finally, Section 7 provides a conclusion to this article.

EXISTENCE CONDITIONS AND FIXED POINT'S STABILITY ANALYSIS

Existence of Fixed points

A quick algebraic calculation reveals that the proposed system (7) has two fixed points for any value of the permitted parameters:

(i) The fixed point of the boundary $E_1(k,0)$. According to biology, when there are no predators, the population of prey achieves its carrying limit k.

(ii) If $0 < d < 1$, then the unique coexistence fixed point $E_2(x^*,y^*)$ exists, where $x^* = -\frac{1}{a}\ln[1-d], y^* = -\frac{r\ln[1-d]\ln[-\frac{ak}{\ln[1-d]}]}{ad}$.

Analysis of local stability for fixed points

At fixed points obtained in section 2.1, we examine the system's stability of the system (7). The magnitude of the eigenvalues calculated at the fixed point $E(x^*,y^*)$, it should be noted that estimated eigenvalues affect the fixed point's local stability.

Then

$$J(x^*,y^*) = \begin{pmatrix} \tilde{j_{11}} & \tilde{j_{12}} \\ \tilde{j_{21}} & \tilde{j_{22}} \end{pmatrix} \tag{8}$$

where

$$\tilde{j_{11}} = 1 - \left(r + ay^*e^{-ax^*} - r\ln[\frac{k}{x^*}]\right)\frac{\rho^\alpha}{\Gamma(\alpha+1)},$$
$$\tilde{j_{12}} = \left(-1 + e^{-ax^*}\right)\frac{\rho^\alpha}{\Gamma(\alpha+1)},$$
$$\tilde{j_{21}} = ay^*e^{-ax^*}\frac{\rho^\alpha}{\Gamma(\alpha+1)},$$
$$\tilde{j_{22}} = 1 + \left(1 - d - e^{-ax^*}\right)\frac{\rho^\alpha}{\Gamma(\alpha+1)}.$$

The Jacobian Matrix's characteristic polynomial can be expressed as follows:

$$F(\lambda) := \lambda^2 + \widehat{p_{ee}}(x,y)\lambda + \widehat{q_{ee}}(x,y) = 0 \tag{9}$$

where $\widehat{p_{ee}}(x,y) = -(\tilde{j_{11}} + \tilde{j_{22}})$ and $\widehat{q_{ee}}(x,y) = \tilde{j_{11}}\tilde{j_{22}} - \tilde{j_{12}}\tilde{j_{21}}$. The following stability conditions of fixed points are stated based on the concept of the Jury's criterion.

The Jacobian matrix (8) at $E_1(k,0)$ can be found as

$$J(E_1) = \begin{pmatrix} 1 - r\frac{\rho^\alpha}{\Gamma(\alpha+1)} & (-1+e^{-ak})\frac{\rho^\alpha}{\Gamma(\alpha+1)} \\ 0 & 1 + \left(1 - d - e^{-ak}\right)\frac{\rho^\alpha}{\Gamma(\alpha+1)} \end{pmatrix} \tag{10}$$

The eigenvalues are $\lambda_1 = 1 - r\frac{\rho^\alpha}{\Gamma(\alpha+1)}$ and $\lambda_2 = 1 + \left(1 - d - e^{-ak}\right)\frac{\rho^\alpha}{\Gamma(\alpha+1)}$

The following topological categorization is valid for the predator-free equilibrium point $E_1(k,0)$:

(a) if $d > (1 - e^{-ak})$ then $E_1(k,0)$ is
- sink if $0 < \rho < min\{\left(\frac{2}{r}\Gamma(1+\alpha)\right)^{\frac{1}{\alpha}}, \left(\frac{2}{d-(1-e^{-ak})}\Gamma(1+\alpha)\right)^{\frac{1}{\alpha}}\}$
- source if $\rho > max\{\left(\frac{2}{r}\Gamma(1+\alpha)\right)^{\frac{1}{\alpha}}, \left(\frac{2}{d-(1-e^{-ak})}\Gamma(1+\alpha)\right)^{\frac{1}{\alpha}}\}$
- non-hyperbolic if $\rho = \left(\frac{2}{r}\Gamma(1+\alpha)\right)^{\frac{1}{\alpha}}$ or $\rho = \left(\frac{2}{d-(1-e^{-ak})}\Gamma(1+\alpha)\right)^{\frac{1}{\alpha}}$

(b) if $d < (1 - e^{-ak})$ then the fixed point $E_1(k,0)$ is
- source if $\rho > \left(\frac{2}{r}\Gamma(1+\alpha)\right)^{\frac{1}{\alpha}}$
- saddle if $\rho < \left(\frac{2}{r}\Gamma(1+\alpha)\right)^{\frac{1}{\alpha}}$
- non-hyperbolic if $\rho = \left(\frac{2}{r}\Gamma(1+\alpha)\right)^{\frac{1}{\alpha}}$

(c) if $d = (1 - e^{-ak})$ then the fixed point $E_1(k,0)$ is non-hyperbolic

Naturally, one of the eigenvalues of the above mentioned jacobian matrix is -1, and the remaining eigenvalues are different from ± 1 when $\rho = \left(\frac{2}{r}\Gamma(1+\alpha)\right)^{\frac{1}{\alpha}}$ or $\rho = \left(\frac{2}{d-(1-e^{-ak})}\Gamma(1+\alpha)\right)^{\frac{1}{\alpha}}$.

Therefore, if parameters change in a limited area around $\widehat{PDF}^1_{E_1}$ or $\widehat{PDF}^2_{E_1}$, a flip bifurcation may happen.

$$\widehat{PDF}^1_{E_1} = \{(r,a,k,d,\rho,\alpha) \in (0,+\infty) : \rho = \left(\frac{2}{r}\Gamma(1+\alpha)\right)^{\frac{1}{\alpha}},$$
$$\rho \neq \left(\frac{2\Gamma(1+\alpha)}{d-(1-e^{-ak})}\right)^{\frac{1}{\alpha}}, d > (1 - e^{-ak})\}$$

or

$$\widehat{PDF}^2_{E_1} = \{(r,a,k,d,\rho,\alpha) \in (0,+\infty) : \rho = \left(\frac{2\Gamma(1+\alpha)}{d-(1-e^{-ak})}\right)^{\frac{1}{\alpha}},$$

$$\rho \neq \left(\tfrac{2}{r}\Gamma(1+\alpha)\right)^{\frac{1}{\alpha}}, d > (1-e^{-ak})\}$$

At $E_2(x^*,y^*)$, the characteristic equation can be written as

$$F_e(\lambda) := \lambda^2 - (2+\tilde{M}_a\tilde{\mu_e})\lambda + (1+\tilde{M}_a\tilde{\mu_e} + \tilde{N}_a\tilde{\mu_e}^2) = 0 \qquad (11)$$

where

$$\tilde{\mu_e} = \frac{\rho^\alpha}{\Gamma(\alpha+1)}$$

$$\tilde{M}_a = e^{-ax^*}\left(-1-e^{ax^*}(-1+d+r) - ay^*\right) + r\ln[\frac{k}{r}]$$

$$\tilde{N}_a = e^{-ax^*}\left(r - e^{ax^*}r(1-d) + ady^* - (1+(-1+d)e^{ax^*})r\ln[\frac{k}{x}]\right)$$

So $F_e(1) = \tilde{M}_a\tilde{\mu_e}^2 > 0$ and $F_e(-1) = 4 + 2\tilde{M}_a\tilde{\mu_e} + \tilde{N}_a\tilde{\mu_a}^2$. Regarding the stability criterion of E_2, we state the following lemma.

The fixed point E_2 with any arbitrary selection of parameter values is a

(i) source if

$(i.i)$ $\tilde{M_a}^2 - 4\tilde{N_a} \geq 0$ and $\tilde{\mu_e} > \frac{-\tilde{M_a}+\sqrt{\tilde{N_a}^2-4\tilde{N_a}}}{\tilde{N_a}}$

$(i.ii)$ $\tilde{M_a}^2 - 4\tilde{N_a} < 0$ and $\tilde{\mu_e} > \frac{-\tilde{M_a}}{\tilde{N_a}}$

(ii) sink if

$(ii.i)$ $\tilde{M_a}^2 - 4\tilde{N_a} \geq 0$ and $\tilde{\mu_e} < \frac{-\tilde{M_a}-\sqrt{\tilde{N_a}^2-4\tilde{N_a}}}{\tilde{N_a}}$

$(ii.ii)$ $\tilde{M_a}^2 - 4\tilde{N_a} < 0$ and $\tilde{\mu_e} < \frac{-\tilde{M_a}}{\tilde{N_a}}$

(iii) non-hyperbolic if

$(iii.i)$ $\tilde{M_a}^2 - 4\tilde{N_a} \geq 0$ and $\tilde{\mu_e} = \frac{-\tilde{M_a}\pm\sqrt{\tilde{M_a}^2-4\tilde{N_a}}}{\tilde{N_a}}; \tilde{\mu_e} \neq \frac{-2}{\tilde{M_a}}, \frac{-4}{\tilde{M_a}}$

$(iii.ii)$ $\tilde{M_a}^2 - 4\tilde{N_a} < 0$ and $\tilde{\mu_e} = \frac{-4}{\tilde{M_a}}$.

(iv) saddle if otherwise

Let,

$$\widehat{PD}_{E_2} = \left\{(r,a,k,d,\rho,\alpha) : \rho = \left(\frac{-\tilde{M_a}\pm\sqrt{\tilde{M_a}^2-4\tilde{N_a}}}{\tilde{N_a}}\Gamma(1+\alpha)\right)^{\frac{1}{\alpha}} = \rho_\pm,\right\}$$

with $\tilde{M_a}^2 - 4\tilde{N_a} \geq 0, \tilde{\mu_e} \neq \frac{-2}{\tilde{M_a}}, \frac{-4}{\tilde{M_a}}$

The system (7) at E_2 undergoes a flip bifurcation, when the parameters (r,a,k,d,ρ,α) fluctuate within a narrow region of $\widehat{PD}_{E_2}$.

Also, let

$$\widehat{NS}_{E_2} = \left\{(r,a,k,d,\rho,\alpha) : \rho = \left(\Gamma(1+\alpha)\frac{-\tilde{M_a}}{\tilde{N_a}}\right)^{\frac{1}{\alpha}} = \rho_{NS}, \tilde{M_a}^2 - 4\tilde{N_a} < 0\right\}$$

If the parameters (r,a,k,d,ρ,α) vary around the set $\widehat{NS}_{E_2}$, system (7) will suffer an NS bifurcation at that point.

BIFURCATION ANALYSIS

This section introduces to investigate the Neimark–Sacker (NS) bifurcation and Period-Doubling (PD) bifurcation at the equilibrium point $E_2\,(x^*,y^*)$ of the system taking ρ as the parameter of bifurcation for this study.

Neimark–Sacker bifurcation

For the formulated predator-prey system (7) in discrete fractional, the bifurcation analysis of the research of Gompertz growth on prey with exposure to Ivlev functional response has been conducted through the NS bifurcation. For the parameters that fall under the following set:

$$\widehat{NS}_{E_2} = \left\{(r,a,k,d,\rho,\alpha) : \rho = \left(\Gamma(1+\alpha)\frac{A_{1e}}{A_{2e}}\right) = \rho_{NS}, \mathfrak{L} < 0\right\},$$

Let ρ^* is the perturbation of ρ where $|\rho^*| \lll 1$. Therefore, the model perturbation is

$$\begin{aligned} x_{n+1} &= x_n + \frac{(\rho+\rho^*)^\alpha}{\Gamma(\alpha+1)}\left(rx_n\ln\frac{k}{x_n} - (1-e^{-ax_n})\,y_n\right) \equiv f(x_n,y_n,\rho^*), \quad (12)\\ y_{n+1} &= y_n + \frac{(\rho+\rho^*)^\alpha}{\Gamma(\alpha+1)}\left((1-e^{-ax_n})\,y_n - dy_n\right) \equiv g(x_n,y_n,\rho^*). \end{aligned}$$

If $u_n = x_n - x^*, v_n = y_n - y^*$, then equilibrium is $E_2\,(x^*,y^*)$ becomes the origin , and by using Taylor series at $(u_n,v_n) = (0,0)$ expanding f and g to the third order, the model (12) becomes

$$\begin{aligned} u_{n+1} &= \alpha_1u_n + \alpha_2v_n + \alpha_{11}u_n^2 + \alpha_{12}u_nv_n + \alpha_{22}v_n^2 + \alpha_{111}u_n^3 + \quad (13)\\ &\quad \alpha_{112}u_n^2v_n + \alpha_{122}u_nv_n^2 + \alpha_{222}v_n^3 + O((|u_n|+|v_n|)^4),\\ v_{n+1} &= \beta_1u_n + \beta_2v_n + \beta_{11}u_n^2 + \beta_{12}u_nv_n + \beta_{22}v_n^2 + \beta_{111}u_n^3 +\\ &\quad \beta_{112}u_n^2v_n + \beta_{122}u_nv_n^2 + \beta_{222}v_n^3 + O((|u_n|+|v_n|)^4), \end{aligned}$$

where

$$\begin{aligned} \alpha_1 &= \frac{d - dr\frac{\rho^\alpha}{\Gamma(\alpha+1)} + r\frac{\rho^\alpha}{\Gamma(\alpha+1)}\left(d-(-1+d)\ln[1-d]\right)\ln\left[\frac{-ak}{\ln[1-d]}\right]}{d},\\ \alpha_2 &= -d\frac{\rho^\alpha}{\Gamma(\alpha+1)},\\ \alpha_{11} &= \frac{ar\frac{\rho^\alpha}{\Gamma(\alpha+1)}\left(d+(-1+d)\ln[1-d]^2\ln\left[\frac{-ak}{\ln[1-d]}\right]\right)}{d\ln[1-d]},\\ \alpha_{12} &= a(-1+d)\frac{\rho^\alpha}{\Gamma(\alpha+1)},\\ \alpha_{22} &= 0,\\ \alpha_{111} &= \frac{a^2r\frac{\rho^\alpha}{\Gamma(\alpha+1)}\left(1-\frac{(-1+d)\ln[1-d]^3\ln\left[\frac{-ak}{\ln[1-d]}\right]}{\ln[1-d]^2}\right)}{\ln[1-d]^2},\\ \alpha_{112} &= -a^2(-1+d)\frac{\rho^\alpha}{\Gamma(\alpha+1)},\\ \alpha_{122} &= 0,\\ \alpha_{222} &= 0,\\ \beta_1 &= \frac{(-1+d)r\frac{\rho^\alpha}{\Gamma(\alpha+1)}\ln[1-d]\ln\left[\frac{-ak}{\ln[1-d]}\right]}{d},\\ \beta_2 &= 1,\\ \beta_{11} &= -\frac{a(-1+d)r\frac{\rho^\alpha}{\Gamma(\alpha+1)}\ln[1-d]\ln\left[\frac{-ak}{\ln[1-d]}\right]}{d},\\ \beta_{22} &= 0,\\ \beta_{111} &= \frac{a^2(-1+d)r\frac{\rho^\alpha}{\Gamma(\alpha+1)}\ln[1-d]\ln\left[\frac{-ak}{\ln[1-d]}\right]}{d},\\ \beta_{112} &= a^2(-1+d)\frac{\rho^\alpha}{\Gamma(\alpha+1)},\\ \beta_{122} &= 0,\\ \beta_{222} &= 0. \end{aligned} \qquad (14)$$

The characteristic equation of the model (13) is $\lambda^2 + p(\rho^*)\lambda + q(\rho^*) = 0$,
where

$$p(\rho^*) = -\frac{d(2-r\frac{(\rho+\rho^*)^\alpha}{\Gamma(\alpha+1)})+r\frac{(\rho+\rho^*)^\alpha}{\Gamma(\alpha+1)}(d-(-1+d)\ln[1-d])\ln[\frac{-ak}{\ln[1-d]}]}{d},$$

and

$$q(\rho^*) = \frac{d(1-r\frac{(\rho+\rho^*)^\alpha}{\Gamma(\alpha+1)})+r\frac{(\rho+\rho^*)^\alpha}{\Gamma(\alpha+1)}\left(d+(-1+d)(-1+d\frac{(\rho+\rho^*)^\alpha}{\Gamma(\alpha+1)})\ln[1-d]\right)\ln[\frac{-ak}{\ln[1-d]}]}{d}.$$

The roots of the characteristic equation are $\lambda_{1,2}(\rho^*) = \frac{-p(\rho^*)\pm i\sqrt{4q(\rho^*)-(p(\rho^*))^2}}{2}$.

where

$$\begin{aligned}
&4q(\rho^*)-(p(\rho^*))^2 \\
&= \frac{4\left(d-dr\frac{(\rho+\rho^*)^\alpha}{\Gamma(\alpha+1)}+r\frac{(\rho+\rho^*)^\alpha}{\Gamma(\alpha+1)}\left(d+(-1+d)(-1+d\frac{(\rho+\rho^*)^\alpha}{\Gamma(\alpha+1)})\ln[1-d]\right)\ln\left[\frac{-ak}{\ln[1-d]}\right]\right)}{d} \\
&- \frac{\left(d(2-r\frac{(\rho+\rho^*)^\alpha}{\Gamma(\alpha+1)})+r\frac{(\rho+\rho^*)^\alpha}{\Gamma(\alpha+1)}(d-(-1+d)\ln[1-d])\ln[\frac{-ak}{\ln[1-d]}]\right)^2}{d^2}
\end{aligned}$$

For $0 < d < 1$, $4q(\rho^*) - (p(\rho^*))^2$ is always less than zero.

From $|\lambda_{1,2}(\rho^*)| = 1$, and $\rho^* = 0$, we have $|\lambda_{1,2}(\rho^*)| = [q(\rho^*)]^{\frac{1}{2}}$ and

$$\begin{aligned}
l &= \left[\frac{d|\lambda_{1,2}(\rho^*)|}{d\rho^*}\right]_{\rho^*=0} \\
&= \frac{r\left(-d+(d+(-1+d)(-1+2d\frac{\rho^\alpha}{\Gamma(\alpha+1)})\ln[1-d])\ln\left[\frac{-ak}{\ln[1-d]}\right]\right)}{2d\sqrt{\frac{d-dr\frac{\rho^\alpha}{\Gamma(\alpha+1)}+r\frac{\rho^\alpha}{\Gamma(\alpha+1)}\left(d+(-1+d)(1+d\frac{\rho^\alpha}{\Gamma(\alpha+1)})\ln[1-d]\right)\ln\left[\frac{-ak}{\ln[1-d]}\right]}{d}}} \neq 0.
\end{aligned}$$

Additionally, it is necessary that when $\rho^* = 0$, $\lambda_{1,2}^i \neq 1$, $i = 1,2,3,4$, which is equivalent to $p(0) \neq \pm 2, 0, 1$.

For normal form study, let $\gamma = Im(\lambda_{1,2})$ and $\delta = Re(\lambda_{1,2})$. We define $T = \begin{bmatrix} 0 & 1 \\ \gamma & \delta \end{bmatrix}$, and using the transformation $\begin{bmatrix} u_n \\ v_n \end{bmatrix} = T \begin{bmatrix} \overline{x}_n \\ \overline{y}_n \end{bmatrix}$, the model (13) becomes

$$\begin{aligned}
\overline{x}_{n+1} &= \delta\overline{x}_n - \gamma\overline{y}_n + f_{11}(\overline{x}_n, \overline{y}_n), \\
\overline{y}_{n+1} &= \gamma\overline{x}_n + \delta\overline{y}_n + g_{11}(\overline{x}_n, \overline{y}_n),
\end{aligned} \tag{17}$$

where the variables $(\overline{x}_n, \overline{y}_n)$ with the order at least two are denoted the terms in the model (17) by the functions f_{11} and g_{11}, respectively.

The following discriminatory amount Ω must be nonzero in order to undergo NSB:

$$\Omega = -Re\left[\frac{(1-2\overline{\lambda})\overline{\lambda}^2}{1-\lambda}\xi_{11}\xi_{20}\right] - \frac{1}{2}|\xi_{11}|^2 - |\xi_{02}|^2 + Re(\overline{\lambda}\xi_{21}),$$

where

$$\begin{aligned}
\xi_{20} &= \frac{\delta}{8}(2\beta_{22} - \delta\alpha_{22} - \alpha_{12} + 4\gamma\alpha_{22} + i(4\gamma\alpha_{22} - 2\alpha_{22} - 2\delta\alpha_{22})) \\
&+ \frac{\gamma}{4}\alpha_{12} + \frac{\beta_{12}}{8} + \frac{\delta\alpha_{11} - 2\beta_{11} + \delta^3\alpha_{22} - \delta^2\beta_{22} - \delta^2\alpha_{12} + \delta\beta_{12}}{4\gamma}, \\
&+ i\frac{1}{8}\left(4\gamma\beta_{22} + 2\gamma^2\alpha_{22} - 2\alpha_{11}\right) \\
\xi_{11} &= \frac{\gamma}{2}(\beta_{22} - \delta\alpha_{22}) + i\frac{1}{2}(\gamma^2\alpha_{22} + \alpha_{11} + \delta\alpha_{12} + \delta^2\alpha_{22}) \\
&+ \frac{\beta_{11} - \delta\alpha_{11} + \delta\beta_{12} - \delta^2\alpha_{12} - 2\delta^2\beta_{22} + 2\delta^3\alpha_{22}}{2\gamma},
\end{aligned} \tag{15}$$

$$\begin{aligned}
\xi_{02} &= \frac{1}{4}\gamma(2\delta\alpha_{22} + \alpha_{12} + \beta_{22}) + i\frac{1}{4}(\beta_{12} + 2\delta\beta_{22} - 2\delta\alpha_{12} - \alpha_{11}) \\
&- \frac{\beta_{11} - \delta\alpha_{11} + \delta\beta_{12} - \delta^2\alpha_{12} + \delta^2\beta_{22} - \delta^3\alpha_{22}}{4\gamma} + \frac{1}{4}\alpha_{22}i(\gamma^2 - 3\delta^2),
\end{aligned}$$

$$\begin{aligned}
\xi_{21} &= \frac{3}{8}\beta_{222}(\gamma^2 + \delta^2) + \frac{\beta_{112}}{8} + \frac{\delta}{4}\alpha_{112} + \frac{\delta}{4}\beta_{122} + \alpha_{122}(\frac{\gamma^2}{8} + \frac{3\delta^2}{8} - \frac{\delta}{4}) \\
&+ \frac{3}{8}\alpha_{111} + i\frac{3}{8}\alpha_{222}(\gamma^2 + 2\delta^2) + i\frac{3\gamma\delta}{8}\alpha_{122} - \frac{1}{8}\beta_{122}\gamma i - i\frac{3\gamma\delta}{8}\beta_{222} \\
&- i\frac{3\beta_{111} - 3\delta\alpha_{111}}{8\gamma} - i\frac{3\delta\beta_{112} - 3\delta^2\alpha_{112}}{8\gamma} - i\frac{3\delta^2\beta_{122} - 3\delta^3\alpha_{122}}{8\gamma} \\
&- i\frac{3\delta^3\beta_{222} - 3\delta^4\alpha_{222}}{8\gamma}.
\end{aligned} \tag{16}$$

The following theorem can be used to demonstrate the direction and stability of the NS bifurcation in light of the explanation above.

If $\Omega \neq 0$, the system undergoes NS bifurcation at E_2 for the parameter ρ varies in neighborhood of $\widehat{NS}_{E_2}$. If $\Omega < 0$ ($\Omega > 0$), then there is a smooth closed invariant curve that can bifurcate from the positive fixed point E_2, and the bifurcation is sub-critical (resp. super-critical).

Period-Doubling bifurcation

The one eigenvalue is $\lambda_1 = -1$ of the positive fixed point $E_2(x^*, y^*)$, and the other one (λ_2) neither 1 nor -1, if the following set contains the model's parameters

$$\widehat{PD}_{E_2} = \left\{(r, a, k, d, \rho, \alpha) : \rho = \left(\Gamma(1+\alpha)\frac{A_{1e} \pm \sqrt{\mathfrak{L}}}{A_{2e}}\right)^{\frac{1}{\alpha}} = \rho_\pm, \mathfrak{L} \geq 0\right\}.$$

Here, we address the PD bifurcation of the system at $E_2(x^*, y^*)$ when a limited fluctuation of parameters in the area of $\widehat{PD}_{E_2}$. The parameter (ρ) is utilized to analyze the NS bifurcation.

Let ρ^* ($|\rho^*| \lll 1$,) is the perturbation of ρ and taking a model perturbation like this

$$\begin{aligned}
x_{n+1} &= x_n + \frac{(\rho+\rho^*)^\alpha}{\Gamma(\alpha+1)}\left(rx_n\ln\frac{k}{x_n} - (1-e^{-ax_n})y_n\right) \equiv f(x_n, y_n, \rho^*), \\
y_{n+1} &= y_n + \frac{(\rho+\rho^*)^\alpha}{\Gamma(\alpha+1)}((1-e^{-ax_n})y_n - dy_n) \equiv g(x_n, y_n, \rho^*).
\end{aligned} \tag{18}$$

If $u_n = x_n - x^*, v_n = y_n - y^*$, then equilibrium $E_2(x^*, y^*)$ is becomes the origin, and by using Taylor series about $(u_n, v_n) = (0,0)$ expanding to the third order of f and g, the model (18) becomes

$$\begin{aligned}
u_{n+1} &= \alpha_1 u_n + \alpha_2 v_n + \alpha_{11}u_n^2 + \alpha_{12}u_n v_n + \alpha_{13}u_n\rho^* + \\
&\alpha_{23}v_n\rho^* + \alpha_{111}u_n^3 + \alpha_{112}u_n^2 v_n + \alpha_{113}u_n^2\rho^* + \\
&\alpha_{123}u_n v_n\rho^* + O((|u_n| + |v_n| + |\rho^*|)^4), \\
v_{n+1} &= \beta_1 u_n + \beta_2 v_n + \beta_{11}u_n^2 + \beta_{12}u_n v_n + \beta_{22}v_n^2 + \beta_{13}u_n\rho^* + \\
&\beta_{23}v_n\rho^* + \beta_{111}u_n^3 + \beta_{112}u_n^2 v_n + \beta_{113}u_n^2\rho^* + \beta_{123}u_n v_n\rho^* + \\
&\beta_{223}v_n^2\rho^* + O((|u_n| + |v_n| + |\rho^*|)^4),
\end{aligned} \tag{19}$$

where

$$
\begin{aligned}
\alpha_{13} &= -\frac{r\left(d+(-d+(-1+d)\ln[1-d])\ln\left[\frac{-ak}{\ln[1-d]}\right]\right)}{d}\frac{\alpha\rho^{\alpha-1}}{\Gamma(\alpha+1)},\\
\alpha_{23} &= -d\frac{\alpha\rho^{\alpha-1}}{\Gamma(\alpha+1)},\\
\alpha_{113} &= \frac{ar\left(d+(-1+d)\ln[1-d]^2\ln\left[\frac{-ak}{\ln[1-d]}\right]\right)}{d\ln[1-d]}\frac{\alpha\rho^{\alpha-1}}{\Gamma(\alpha+1)},\\
\alpha_{123} &= a(-1+d)\frac{\alpha\rho^{\alpha-1}}{\Gamma(\alpha+1)},\\
\beta_{13} &= \frac{(-1+d)r\ln[1-d]\ln\left[\frac{-ak}{\ln[1-d]}\right]}{d}\frac{\alpha\rho^{\alpha-1}}{\Gamma(\alpha+1)},\\
\beta_{23} &= 0,\\
\beta_{113} &= -\frac{a(-1+d)r\ln[1-d]\ln\left[\frac{-ak}{\ln[1-d]}\right]}{d}\frac{\alpha\rho^{\alpha-1}}{\Gamma(\alpha+1)},\\
\beta_{123} &= a(1-d)\frac{\alpha\rho^{\alpha-1}}{\Gamma(\alpha+1)},\\
\beta_{223} &= 0.
\end{aligned}
\tag{20}
$$

We define $T=\begin{bmatrix}\alpha_2 & \alpha_2\\ -1-\alpha_1 & \lambda_2-\alpha_1\end{bmatrix}$ which is invertible. Now, applying the transformation $\begin{bmatrix}u_n\\ v_n\end{bmatrix}=T\begin{bmatrix}\bar{x}_n\\ \bar{y}_n\end{bmatrix}$, the system (19) becomes

$$
\begin{aligned}
\bar{x}_{n+1} &= -\bar{x}_n+f_{11}(u_n,v_n,b^*),\\
\bar{y}_{n+1} &= \lambda_2\bar{y}_n+g_{11}(u_n,v_n,b^*),
\end{aligned}
\tag{21}
$$

where the variables $(\bar{x}_n,\bar{y}_n)$ having the order at least two are denoted the terms in the model (21) by the functions f_{11} and g_{11}, respectively.

Using the center manifold theorem, it can be derived that the system (21) has a center manifold $W^c(0,0,0)$ at $(0,0)$ in a very closed neighbourhood of $\rho^*=0$, which may roughly be stated as follows:

$W^c(0,0,0)=\{(\bar{x}_n,\bar{y}_n,\rho^*)\,\epsilon R^3:\bar{y}_{n+1}=\bar{\alpha}_1\bar{x}_n^2+\bar{\alpha}_2\bar{x}_n\rho^*$
$+O((|\bar{x}_n|+|\rho^*|)^3)\}$

$$
\begin{aligned}
\bar{\alpha}_1 &= \frac{\alpha_2[(1+\alpha_1)\alpha_{11}+\alpha_2\beta_{11}]}{1-\lambda_2^2}+\frac{\beta_{22}(1+\alpha_1)^2}{1-\lambda_2^2}-\\
&\quad\frac{(1+\alpha_1)[\alpha_{12}(1+\alpha_1)+\alpha_2\beta_{12}]}{1-\lambda_2^2},\\
\bar{\alpha}_2 &= \frac{(1+\alpha_1)[\alpha_{23}(1+\alpha_1)+\alpha_2\beta_{23}]}{\alpha_2(1+\lambda_2)^2}-\frac{(1+\alpha_1)\alpha_{13}+\alpha_2\beta_{13}]}{(1+\lambda_2)^2}.
\end{aligned}
$$

The center manifold $W^c(0,0,0)$ restricted the model (21) has the following form:

$\bar{x}_{n+1} = -\bar{x}_n+h_1\bar{x}_n^2+h_2\bar{x}_n\rho^*+h_3\bar{x}_n^2\rho^*+h_4\bar{x}_n\rho^{*2}+h_5\bar{x}_n^3+O((|\bar{x}_n|+|\rho^*|)^3)\equiv F(\bar{x}_n,\rho^*)$

where

$$
\begin{aligned}
h_1 &= \frac{\bar{\alpha}_2[(\lambda_2-\bar{\alpha}_1)\alpha_{11}-\bar{\alpha}_2\beta_{11}]}{1+\lambda_2}-\frac{\beta_{22}(1+\bar{\alpha}_1)^2}{1+\lambda_2}-\\
&\quad\frac{(1+\bar{\alpha}_1)[(\lambda_2-\bar{\alpha}_1)\alpha_{12}-\bar{\alpha}_2\beta_{12}]}{1+\lambda_2},\\
h_2 &= \frac{(\lambda_2-\bar{\alpha}_1)\alpha_{13}-\bar{\alpha}_2\beta_{13}}{1+\lambda_2}-\frac{(1+\bar{\alpha}_1)[(\lambda_2-\bar{\alpha}_1)\alpha_{23}-\bar{\alpha}_2\beta_{23}]}{\bar{\alpha}_2(1+\lambda_2)},\\
h_3 &= \frac{(\lambda_2-\alpha_1)\bar{\alpha}_1\alpha_{13}-\alpha_2\beta_{13}}{1+\lambda_2}+\frac{[(\lambda_2-\alpha_1)\alpha_{23}-\alpha_2\beta_{23}](\lambda_2-\alpha_1)\bar{\alpha}_1}{\alpha_2(1+\lambda_2)}-\\
&\quad\frac{(1+\alpha_1)[(\lambda_2-\alpha_1)\alpha_{123}-\alpha_2\beta_{123}]}{1+\lambda_2}+\frac{\alpha_2[(\lambda_2-\alpha_1)\alpha_{113}-\alpha_2\beta_{113}]}{1+\lambda_2}+\\
&\quad\frac{2\alpha_2\bar{\alpha}_2[(\lambda_2-\alpha_1)\alpha_{11}-\alpha_2\beta_{11}]}{1+\lambda_2}-\frac{2\beta_{22}\bar{\alpha}_2(1+\alpha_1)(\lambda_2-\alpha_1)}{1+\lambda_2}-\\
&\quad\frac{\beta_{223}(1+\alpha_1)^2}{1+\lambda_2}+\frac{\bar{\alpha}_2[(\lambda_2-\alpha_1)\alpha_{12}-\alpha_2\beta_{12}](\lambda_2-1-2\alpha_1)}{1+\lambda_2},\\
h_4 &= \frac{\bar{\alpha}_2[(\lambda_2-\alpha_1)\alpha_{13}-\alpha_2\beta_{13}]}{1+\lambda_2}+\frac{[(\lambda_2-\alpha_1)\alpha_{23}-\alpha_2\beta_{23}](\lambda_2-\alpha_1)\bar{\alpha}_2}{\alpha_2(1+\lambda_2)}+\\
&\quad\frac{2\alpha_2\bar{\alpha}_2[(\lambda_2-\alpha_1)\alpha_{11}-\alpha_2\beta_{11}]}{1+\lambda_2}+\frac{2\beta_{22}\bar{\alpha}_2(1+\alpha_1)(\lambda_2-\alpha_1)}{1+\lambda_2}+\\
&\quad\frac{\bar{\alpha}_2[(\lambda_2-\alpha_1)\alpha_{12}-\alpha_2\beta_{12}](\lambda_2-1-2\alpha_1)}{1+\lambda_2},\\
h_5 &= \frac{2\alpha_2\bar{\alpha}_1[(\lambda_2-\alpha_1)\alpha_{11}-\alpha_2\beta_{11}]}{1+\lambda_2}+\frac{2\beta_{22}\bar{\alpha}_1(\lambda_2-\alpha_1)(1+\alpha_1)}{1+\lambda_2}-\\
&\quad\frac{\bar{\alpha}_2(1+\alpha_1)[(\lambda_2-\alpha_1)\alpha_{112}-\alpha_2\beta_{112}]}{1+\lambda_2}+\frac{\bar{\alpha}_2^2[(\lambda_2-\alpha_1)\alpha_{111}-\alpha_2\beta_{111}]}{1+\lambda_2}\\
&\quad+\frac{[(\lambda_2-\alpha_1)\alpha_{11}-\alpha_2\beta_{11}](\lambda_2-1-2\alpha_1)\bar{\alpha}_1}{1+\lambda_2}.
\end{aligned}
$$

For PD bifurcation, the two differentiating quantities ξ_1 and ξ_2 be nonzero,

$\xi_1 = \left(\frac{\partial^2F}{\partial\bar{x}\partial\rho^*}+\frac{1}{2}\frac{\partial F}{\partial\rho^*}\frac{\partial^2F}{\partial\bar{x}^2}\right)\Big|_{(0,0)}$ and $\xi_2 = \left(\frac{1}{6}\frac{\partial^3F}{\partial\bar{x}^3}+\left(\frac{1}{2}\frac{\partial^2F}{\partial\bar{x}^2}\right)^2\right)\Big|_{(0,0)}$.

The following theorem contains a succinct statement of the previously discussed topic.

If $\xi_1\neq 0$ and $\xi_2\neq 0$ then the system undergoes PD bifurcation at $E_2(x^*,y^*)$ for varies of ρ in a small neighborhood of b_{PDB}. Further, the period-two orbits for $\xi_2>0$ ($\xi_2<0$) that bifurcate from $E_2(x^*,y^*)$ is stable (unstable).

EXISTENCE OF MAROTTOS CHAOS

This section presents the condition under which the system (7) will be chaotic in the sense of Marotto (1978, 2005). Fixed point z of system f is repelling if all of the eigenvalues of $Df(z)$ are greater than 1. A repelling fixed point z is snap-back repeller of system f if there is a point $x_0\neq z$ in the repelling vicinity of z, such that $x_M=z$ and $det(Df(x_k))\neq 0$ for $1\leq k\leq M$, where $x_k=f^k(x_0)$. A snap-back repeller indicates that system f is chaotic.

$E_2(x^*,y^*)$ is an repelling fixed point of $F(X_n)$ if $p^2(x^*,y^*)-4q(x^*,y^*)<0$ and $q(x^*,y^*)-1>0$

For map $F(X_n)=\begin{pmatrix}x_n+\frac{\rho^\alpha}{\Gamma(\alpha+1)}\left(rx_n\ln\frac{k}{x_n}-\left(1-e^{-ax_n}\right)y_n\right)\\ y_n+\frac{\rho^\alpha}{\Gamma(\alpha+1)}\left(\left(1-e^{-ax_n}\right)y_n-dy_n\right)\end{pmatrix}$,

$X_n=(x_n\ \ y_n)^T$

The eigenvalues that match the fixed point $E_2(x^*,y^*)$ are given by $\lambda_{1,2}=\frac{-\widehat{p}(x^*,y^*)\pm\sqrt{\widehat{p}^2(x^*,y^*)-4\widehat{q}(x^*,y^*)}}{2}$, where

$\widehat{p}(x^*,y^*) = -(2 - \frac{r\rho^\alpha}{\Gamma(\alpha+1)}) - \frac{r\rho^\alpha}{d\Gamma(\alpha+1)}(d-(-1+d)\ln[1-d])\ln\left[\frac{-ak}{\ln[1-d]}\right]$,

$\widehat{q}(x^*,y^*) = (1 - \frac{r\rho^\alpha}{\Gamma(\alpha+1)}) + \frac{r\rho^\alpha}{d\Gamma(\alpha+1)}(d+(-1+d)(-1+\frac{d\rho^\alpha}{\Gamma(\alpha+1)})\ln[1-d])\ln\left[\frac{-ak}{\ln[1-d]}\right]$.

As a result, the fixed point $E_2(x^*,y^*)$ has two complex eigenvalues, and their norm is greater than unity if

$p^2(x^*,y^*) - 4q(x^*,y^*) < 0$ and $q(x^*,y^*) - 1 > 0$

As a result, we can assert the following inference.

$E_2(x^*,y^*)$ is a snap-back repeller of $F(X_n)$ if $\left|DF^2(E(x_0,y_0))\right| \neq 0$.

Let $E(x_0,y_0) \neq E_2(x^*,y^*)$ be a point in a repelling neighborhood of $E_2(x^*,y^*)$, such that $F^2(E(x_0,y_0)) = E_2(x^*,y^*)$.

Therefore

$$x_1 = x_0 + \frac{\rho^\alpha}{\Gamma(\alpha+1)}\left(rx_0\ln\frac{k}{x_0} - \left(1-e^{-ax_0}\right)y_0\right) \text{ and}$$

$$y_1 = y_0 + \frac{\rho^\alpha}{\Gamma(\alpha+1)}\left(\left(1-e^{-ax_0}\right)y_0 - dy_0\right) \tag{22}$$

and

$$x^* = x_1 + \frac{\rho^\alpha}{\Gamma(\alpha+1)}\left(rx_1\ln\frac{k}{x_1} - \left(1-e^{-ax_1}\right)y_1\right) \text{ and}$$

$$y^* = y_1 + \frac{\rho^\alpha}{\Gamma(\alpha+1)}\left(\left(1-e^{-ax_1}\right)y_1 - dy_1\right). \tag{23}$$

We will calculate the value of x_0 and y_0 by solving equations (22) and (23)

By simple calculations, we get

$$\left|DF^2(E(x_0,y_0))\right| = \left|DF(E(x_0,y_0))\right|\left|DF(F(E(x_0,y_0)))\right|$$

$$= (CH-DG)\begin{bmatrix} 1+\left\{1-d-r-(1+aB)e^{-aA}+r\ln\frac{k}{A}\right\}\frac{\rho^\alpha}{\Gamma(\alpha+1)} \\ +\left\{d(r+aBe^{-aA}-r\ln\frac{k}{A})-r(1-e^{-aA})(1-\ln\frac{k}{A})\right\}\left(\frac{\rho^\alpha}{\Gamma(\alpha+1)}\right)^2 \end{bmatrix}$$

where $A = x_0 + \frac{\rho^\alpha}{\Gamma(\alpha+1)}\left(rx_0\ln\frac{k}{x_0} - \left(1-e^{-ax_0}\right)y_0\right)$, $B = y_0 + \frac{\rho^\alpha}{\Gamma(\alpha+1)}\left(\left(1-e^{-ax_0}\right)y_0 - dy_0\right)$,

$C = 1 - \frac{\rho^\alpha}{\Gamma(\alpha+1)}\left(r + ay_0e^{-ax_0} - r\ln\frac{k}{x_0}\right)$, $D = \frac{\rho^\alpha}{\Gamma(\alpha+1)}\left(-1+e^{-ax_0}\right)$,

$G = \frac{\rho^\alpha}{\Gamma(\alpha+1)}\left(ay_0e^{-ax_0}\right)$, $H = 1 + \frac{\rho^\alpha}{\Gamma(\alpha+1)}\left(1-d-e^{-ax_0}\right)$.

Therefore $E_2(x^*,y^*)$ is a snap-back repeller of $F(X_n)$ when $\left|DF^2(E(x_0,y_0))\right| \neq 0$ Further, the following inference can claim as a result of the chaotic nature. $F(X_n)$ is chaotic under the condition $p^2(x^*,y^*) - 4q(x^*,y^*) < 0$, $q(x^*,y^*) - 1 > 0$ and $\left|DF^2(E(x_0,y_0))\right| \neq 0$. Since $F(X_n)$ has a repelling fixed point $E_2(x^*,y^*)$ if $p^2(x^*,y^*) - 4q(x^*,y^*) < 0$, $q(x^*,y^*) - 1 > 0$, and further from Theorem-5, the same fixed point $E_2(x^*,y^*)$ is a snap-back repeller if $\left|DF^2(E(x_0,y_0))\right| \neq 0$.
Therefore $F(X_n)$ is chaotic.

NUMERICAL SIMULATIONS

The Lyapunov exponent, bifurcation diagram, phase portrait and fractal dimension are shown for various parameter values in this section to illustrate the qualitative dynamical characteristic of the discrete fractional system. To support our theoretical conclusions for the system (7), we shall run numerical simulations. These parameter values were picked: $r = 1.2$, $k = 1.5$, $a = 0.5$, $\alpha = 0.75$, $d = 0.1$ and ρ varies between $1.9 \leq \rho \leq 2.73$. We locate a fixed point $E(x^*,y^*) = (1.02165, 3.36309)$ and assess the bifurcation point for the system (7) at $\rho_- = 2.08616$. The eigenvalues are $\lambda_{1,2} = -1, 0.937016$.

The system trajectory is shown in Figure 2 as changing from a fixed point to a Flip bifurcation and finally to a chaotic attractor. The computed MLEs and FDs associated with Figure 2(a-b) are shown in Figure 2 (c-d). In reference of the bifurcation Figure 2, the phase portraits are displayed in Figure 3, which effectively illustrates the bifurcation of a smooth, invariant closed curve into a chaotic attractor from a stable fixed point.

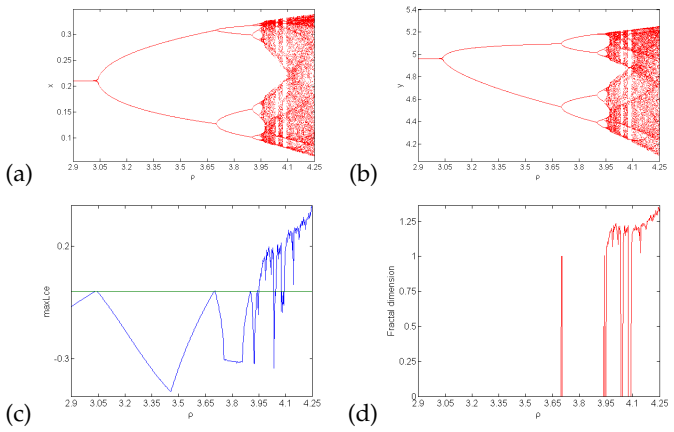

Figure 2 Flip Bifurcation diagram, MLEs and FDs for varying parameter ρ

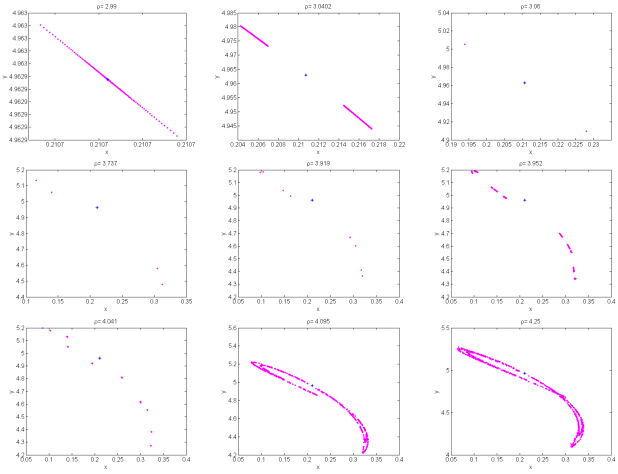

Figure 3 Phase picture for varying ρ with matching to Figure 2 a,b. Blue $*$ is the fixed point E_0.

In Figure 4, the orbit diagram of the prey and predator populations is shown together with other fixed parameter values are $r = 1.2, k = 1.5, a = 1.0, \alpha = 0.5, d = 0.4$ and ρ varies between $2.5 \leq \rho \leq 3.25$. We establish a fixed point $E(x^*,y^*) = (0.510826, 3.30154)$ and assess the bifurcation point for the system (7) at $\rho_{NS} = 2.65984$. The eigenvalues are $\lambda_{1,2} = -0.0173315 \pm 0.99985i$. This figure showing transition of trajectory from a fixed point to NSB and finally to chaotic attractor. The phase portrait, MLEs and FD of Figure 4 (a-b) are shown in Figure 5 and Figure 4 (c-d) respectively. All bifurcation processes for both prey and predator have three distinct periodic windows.

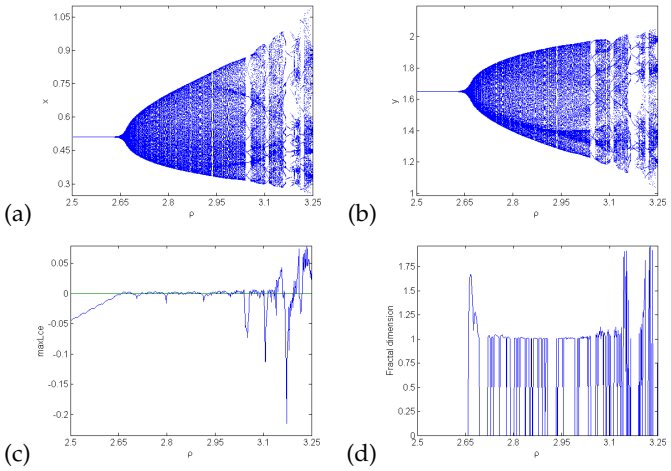

Figure 4 Visual representation of NS Bifurcation, MLEs and FDs of species for varying parameter ρ

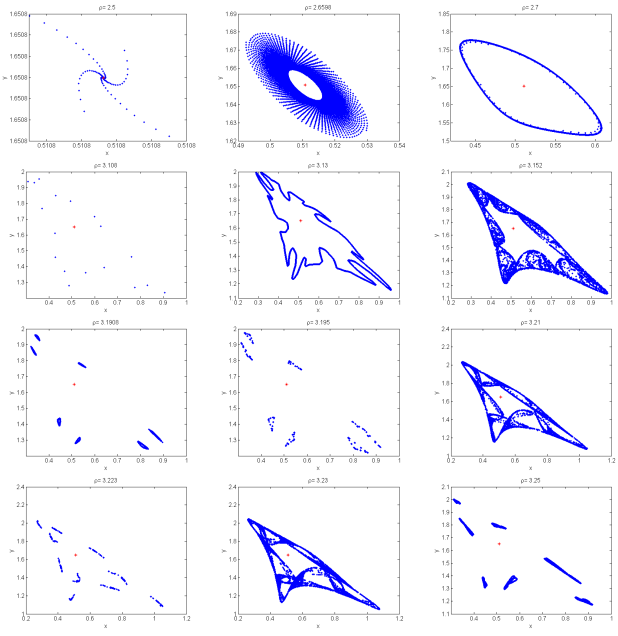

Figure 5 Phase picture for changing input of ρ matching to Figure 4 a,b. Red $*$ is the fixed point E_0.

We have also investigated NS bifurcation by varying the fractional order α in the range $0.65 \leq \alpha \leq 0.985$ and fixed all other parameter discussed above for Figure 4 with $\rho = 2.65984$. The visual representation of Figure 6 is displayed in Figure 7.

The prey-predator model may behave more dynamically in the Neimark-Sacker bifurcation diagram as other parameter values vary (for example, parameter a). When the parameter values are set as $r = 1.2$, $k = 1.5$, $\alpha = 0.75$, $d = 0.4$ with $\rho = 2.65984$ and a range between $0.5 \leq a \leq 1.33$, as illustrated in Figure 8 (a-b), a new Neimark-Sacker bifurcation diagram is produced. At $a = a_{NS} = 1.0$, the system encounters a Neimark-Sacker bifurcation. Figures 9 and 8 (c-d) illustrate, respectively, the phase portrait, MLEs, and FD of Figure 8(a-b). Figure 10 (a) shows the 3D bifurcation diagrams in (ρ, b, x)-space. The plot of the maximal Lyapunov exponents is shown in Figure 10 (b) for two control parameters through a 2D projection onto the (ρ, a) plane.

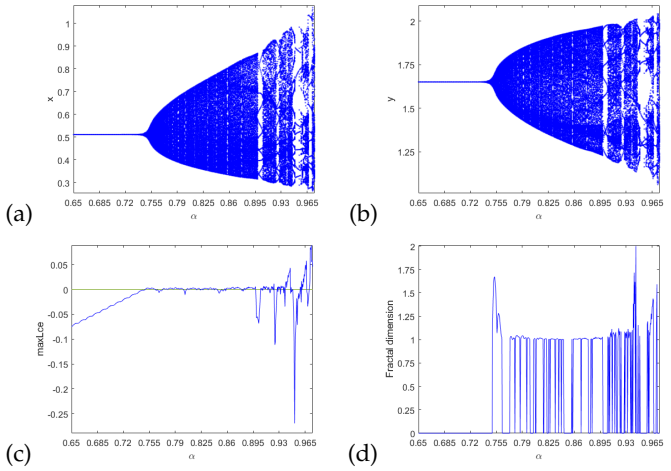

Figure 6 Diagram of NS Bifurcation in (a) (α, x) plane, (b) (α, y) plane, (c) MLEs , (d) FDs

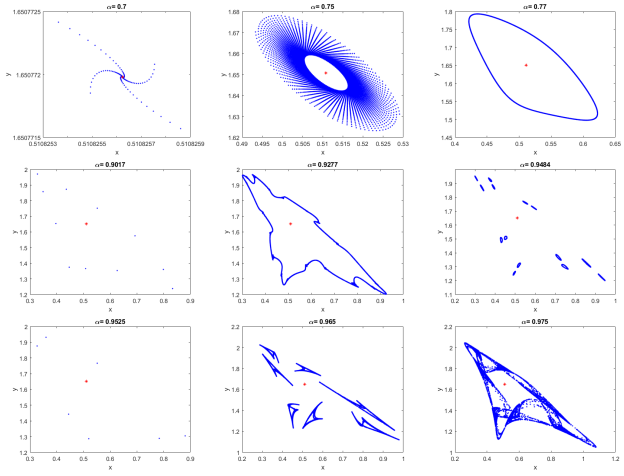

Figure 7 Phase picture for different inputs of α matching to Figure 6 a,b. Red $*$ is the fixed point E_2.

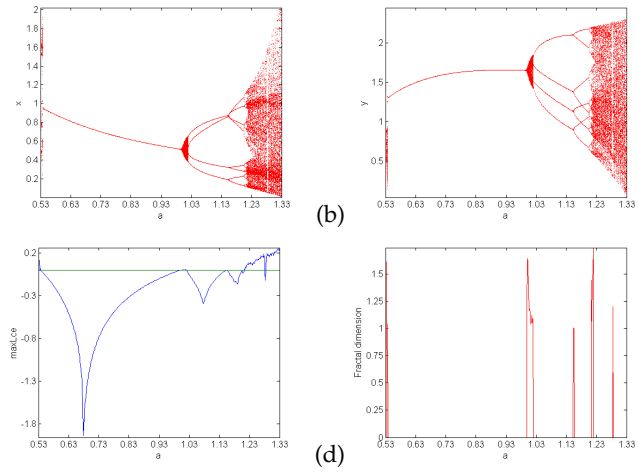

Figure 8 Diagram of NS Bifurcation in (a) (a, x) plane, (b) (a, y) plane, (c) MLEs , (d) FDs

Fractal Dimension

To determine chaotic attractors of a system, the fractal dimensions (FD) measurement is used and is defined by Cartwright (1999)

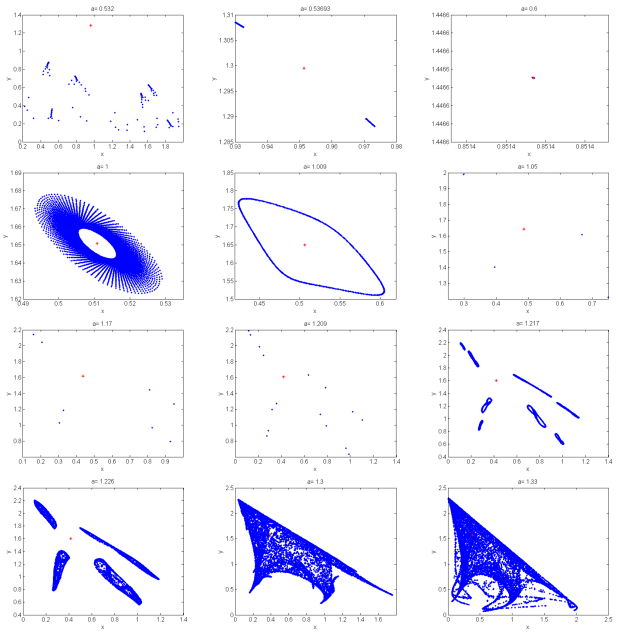

Figure 9 Phase picture for different inputs of a matching to Figure 8 a,b. Red $*$ is the fixed point E_2.

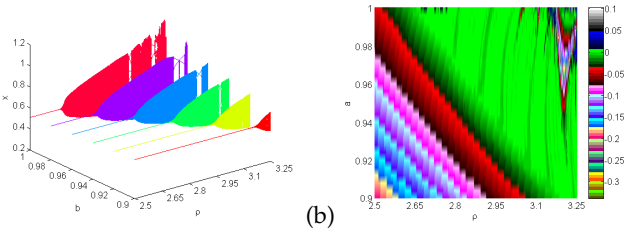

Figure 10 (a) 3D Bifurcation diagram in (ρ, b, x) space (b) Maximum Lyapunov exponents projected in two dimensions onto the (ρ, a) plane

$$\widehat{D}_{FD} = k + \frac{\sum_{j=1}^{k} \mathrm{tt}_j}{|\mathrm{tt}_{k+1}|} \tag{24}$$

where the largest integer is k such that $\sum_{j=1}^{k} \mathrm{tt}_j \geq 0$ and $\sum_{j=1}^{k+1} \mathrm{tt}_j < 0$ and t_j's are Lyapunov exponenets.

Now, the system's fractal dimensions (7) have the following structure:

$$\widehat{D}_{FD} = 2 + \frac{\mathrm{tt}_1}{|\mathrm{tt}_2|} \tag{25}$$

It is certain that the dynamics of the fractional order prey-predator system become unstable as the value of the parameter ρ rises since the chaotic dynamics of the system (7) (ref. Figure 5) are quantified with the sign of FD (ref. Figure 4 (d)).

CHAOS CONTROL

Dynamical systems are thought to be optimal in reference to a performance criterion and will avert chaos. Chaotic behavior is investigated in physics, biology, ecology, telecommunications, and other domains. Additionally, useful chaos management approaches can be used to a wide range of sectors, including communication systems, physics labs, biochemistry, turbulence, and cardiology. The challenge of regulating chaos dynamics in discrete-time systems has recently piqued the interest of many academics.

The four approaches for researching chaos control in discrete-time models most frequently referenced to take the challenge of controlling chaos are the state feedback method, pole-placement methodology, OGY technique, and hybrid control approach. We introduce OGY (Edward *et al.* 1990) and state feedback (Lynch 2007) for managing chaos in the fractional order prey-predator model. We are unable to use ρ as a control parameter in the OGY technique. To implement the OGY approach, a serves as a control parameter.

To apply the OGY approach, we can rewrite the system (7) as shown below.

$$\begin{aligned} x_{n+1} &= x_n + \frac{\rho^{\alpha}}{\Gamma(\alpha+1)}\left(r x_n \ln\frac{k}{x_n} - (1-e^{-a x_n}) y_n\right) = \tilde{f_{e1}}(x,y,a), \\ y_{n+1} &= y_n + \frac{\rho^{\alpha}}{\Gamma(\alpha+1)}\left((1-e^{-a x_n}) y_n - d y_n\right) = \tilde{f_{e2}}(x,y,a) \end{aligned} \tag{26}$$

where a is the parameter for chaos control. Additionally, let us assume that the chaotic regions are defined by $|a - a_0| < \tilde{v}$, where $\tilde{v} > 0$ and a_0 symbolizes the nominal parameter. Our stabilizing feedback control system steers the trajectory toward the desired orbit. If the system (7) has an unstable fixed point at (x^+, y^+) in a chaotic zone created by the development of a Neimark-Sacker bifurcation, the following linear map can represent the system (26) in the vicinity of the unstable fixed point at (x^+, y^+).

$$\begin{bmatrix} x_{n+1} - x^+ \\ y_{n+1} - y^+ \end{bmatrix} \approx \tilde{A_{ee}} \begin{bmatrix} x_n - x^+ \\ y_n - y^+ \end{bmatrix} + \tilde{B_{ee}}\,[a - a_0] \tag{27}$$

where

$$\tilde{A_{ee}} = \begin{bmatrix} \frac{\partial \tilde{f_{e1}}(x,y,a)}{\partial x} & \frac{\partial \tilde{f_{e1}}(x,y,a)}{\partial y} \\ \frac{\partial \tilde{f_{e2}}(x,y,a)}{\partial x} & \frac{\partial \tilde{f_{e2}}(x,y,a)}{\partial y} \end{bmatrix}$$

$$= \begin{bmatrix} 1 + r\tilde{\mu_e}\left(-1 + \ln\frac{k}{x^+} - a\tilde{R_{e1}}\right) & (-1 + e^{-a x^+})\tilde{\mu_e} \\ a r \tilde{\mu_e} \tilde{R_{e1}} & 1 + \tilde{\mu_e}(1 - d - e^{-a x^+}) \end{bmatrix}$$

and

$$\tilde{B_{ee}} = \begin{bmatrix} \frac{\partial \tilde{f_{e1}}(x,y,a)}{\partial a} \\ \frac{\partial \tilde{f_{e2}}(x,y,a)}{\partial a} \end{bmatrix} = \begin{bmatrix} -\tilde{R_{e2}} \\ \tilde{R_{e2}} \end{bmatrix}$$

For convenience, here we let $\frac{\rho^{\alpha}}{\Gamma(\alpha+1)} = \tilde{\mu_e}$, $\tilde{R_{e1}} = \frac{e^{-a x^+} x^+ \ln\frac{-ak}{\ln[1-d]}}{d}$ and $\tilde{R_{e2}} = \frac{e^{-a x^+} r x^{+2} \tilde{\mu_e} \ln\frac{-ak}{\ln[1-d]}}{d}$

The system's (26) controllability matrix, is therefore defined as follows:

$$\tilde{C_{ee}} = [\tilde{B_{ee}} : \tilde{A_{ee}}\tilde{B_{ee}}]$$

$$= \begin{bmatrix} -\tilde{R_{e2}} & \frac{e^{-2a x^+} r x^{+2} \ln\frac{-ak}{\ln[1-d]} \left(d(\tilde{\mu_e} + e^{a x^+}(-1+(-1+r)\tilde{\mu_e}) - d e^{a x^+} r \ln\frac{k}{x^+}) + a r x^+ \tilde{\mu_e} \ln\frac{-ak}{\ln[1-d]}\right)}{d^2} \\ \tilde{R_{e2}} & \frac{e^{-2a x^+} r x^{+2} \ln\frac{-ak}{\ln[1-d]} \left(d(\tilde{\mu_e} + e^{a x^+}(-1+(-1+r)\tilde{\mu_e}) + a r x^+ \tilde{\mu_e} \ln\frac{-ak}{\ln[1-d]}\right)}{d^2} \end{bmatrix}$$

It is then clear to determine that the rank of $\tilde{C_{ee}}$ is 2. Assume that $[a - a_0] = -\tilde{K_{ee}} \begin{bmatrix} x_n - x^+ \\ y_n - y^+ \end{bmatrix}$ where $\tilde{K_{ee}} = [\tilde{\sigma_{e1}} \quad \tilde{\sigma_{e2}}]$, then system (26) becomes

$$\begin{bmatrix} x_{n+1}-x^+ \\ y_{n+1}-y^+ \end{bmatrix} \approx [\tilde{A_{ee}}-\tilde{B_{ee}}\tilde{K_{ee}}] \begin{bmatrix} x_n-x^+ \\ y_n-y^+ \end{bmatrix}$$

Additionally, (7) offers the appropriate controlled system.

$$\begin{aligned} x_{n+1} &= x_n+\tilde{\mu_e}\left(rx_n\ln\frac{k}{x_n}-(1-e^{-(a_0-\tilde{\sigma_{e1}}(x_n-x^+)-\tilde{\sigma_{e2}}(y_n-y^+))x_n})y_n\right)\\ y_{n+1} &= y_n+\tilde{\mu_e}\left((1-e^{-(a_0-\tilde{\sigma_{e1}}(x_n-x^+)-\tilde{\sigma_{e2}}(y_n-y^+))x_n})y_n-dy_n\right) \end{aligned} \tag{28}$$

Additionally, the fixed point (x^+,y^+) is locally asymptotically stable iff both eigenvalues $(\tilde{A_{ee}}-\tilde{B_{ee}}\tilde{K_{ee}})$ of the matrix are situated inside an open unit disk.

Also,

$$\tilde{A_{ee}}-\tilde{B_{ee}}\tilde{K_{ee}}=$$

$$\begin{bmatrix} 1+\tilde{\mu_e}\left(r\ln\frac{k}{x^+}-ar\tilde{R_{e1}}-r\right)+\tilde{R_{e2}}\tilde{\sigma_{e1}} & (e^{-ax^+}-1)\tilde{\mu_e}+\tilde{R_{e2}}\tilde{\sigma_{e2}} \\ ar\tilde{R_{e1}}-\tilde{R_{e2}}\tilde{\sigma_{e1}} & 1+(d-e^{-ax^+}-1)\tilde{\mu_e}-\tilde{R_{e2}}\tilde{\sigma_{e2}} \end{bmatrix}$$

Also

$$\begin{aligned} &\lambda_e{}^2-\left(2+(1-d-e^{ax^+})\tilde{\mu_e}+\tilde{\mu_e}(r\ln\frac{k}{x^+}-r-ar\tilde{R_{e1}})+(\tilde{R_{e2}}\tilde{\sigma_{e1}}-\tilde{R_{e2}}\tilde{\sigma_{e2}})\right)\lambda_e\\ &+\frac{e^{-ax^+}}{d}\left(d\tilde{\mu_e}(r\tilde{\mu_e}-1)+de^{ax^+}(1+\tilde{\mu_e}(1-d-r-r\tilde{\mu_e}(1-d)))\right)\\ &+\frac{1}{d}e^{-ax^+}\left(dr\tilde{\mu_e}\ln\frac{k}{x^+}(e^{x^+}-\tilde{\mu_e}(1-e^{ax^+}(1-d)))\right)+\\ &\frac{e^{-ax^+}}{d}\left(rx^+\tilde{\mu_e}\ln\frac{-ak}{\ln[1-d]}(a\tilde{\mu_e}-a+x^+(1-d\tilde{\mu_e})\tilde{\sigma_{e1}}-x^+(1-r\tilde{\mu_e}+r\tilde{\mu_e}\ln\frac{k}{x^+})\tilde{\sigma_{e2}})\right)=0. \end{aligned} \tag{29}$$

The lines of marginal stability can then be obtained by solving the equations $\lambda_{e1}=\pm1$ and $\lambda_{e1}\lambda_{e2}=1$. Furthermore, these restrictions ensure that the open unit disc has both eigenvalues. Let us consider $\lambda_{e1}\lambda_{e2}=1$ and from (29), we get

$$\begin{aligned} L_{e1} &= \frac{-1}{d}e^{-ax^+}\tilde{\mu_e}\left(d(1-r\tilde{\mu_e})-de^{ax^+}(1-d-r-r\tilde{\mu_e}(1-d))\right)\\ &+\frac{-1}{d}e^{-ax^+}\tilde{\mu_e}\left(dr\ln\frac{k}{x^+}(-e^{ax^+}+\tilde{\mu_e}(1-e^{ax^+}+de^{ax^+}))\right)-\\ &\frac{e^{-ax^+}}{d}\tilde{\mu_e}\left(rx^+\ln\frac{-ak}{\ln[1-d]}(a-ad\tilde{\mu_e}+x^+(1-d\tilde{\mu_e})\tilde{\sigma_{e1}}+x^+(1-r\tilde{\mu_e}+r\tilde{\mu_e}\ln\frac{k}{x^+})\tilde{\sigma_{e2}})\right). \end{aligned}$$

Next, if we assume that $\lambda_{e1}=1$, we obtain

$$\begin{aligned} L_{e2} &= \frac{1}{d}e^{-ax^+}\left(d\tilde{\mu_e}(-2+\tilde{\mu_e})+de^{ax^+}(4+2\tilde{\mu_e}-2d\tilde{\mu_e}-r\tilde{\mu_e}(2+r\tilde{\mu_e}-dr\tilde{\mu_e}))\right)\\ &+\frac{1}{d}e^{-ax^+}\left(dr\tilde{\mu_e}\ln\frac{k}{x^+}(2e^{ax^+}-\tilde{\mu_e}(1-e^{ax^+}-de^{ax^+}))\right)+\\ &\frac{1}{d}e^{-ax^+}\left(rx^+\tilde{\mu_e}\ln\frac{-ak}{\ln[1-d]}(-2a+ad\tilde{\mu_e}+x^+(2-d\tilde{\mu_e})\tilde{\sigma_{e1}}+x^+(-2+r\tilde{\mu_e}-r\tilde{\mu_e}\ln\frac{k}{x^+})\tilde{\sigma_{e2}})\right). \end{aligned}$$

Also, if $\lambda_{e1}=-1$, then

$$\begin{aligned} L_{e3} &= \frac{e^{-ax^+}r\tilde{\mu_e}^2}{d}\left(d(e^{ax^+}-de^{ax^+}-1+(1+(-1+d)e^{ax^+})\ln\frac{k}{x^+}-ax^+\ln\frac{-ak}{\ln[1-d]})\right)\\ &+\frac{1}{d}e^{-ax^+}r\tilde{\mu_e}^2\ln\frac{-ak}{\ln[1-d]}x^{+2}\left(d\tilde{\sigma_{e1}}+r(-1+\frac{k}{x^+}\tilde{\sigma_{e2}})\right). \end{aligned}$$

For a given parametric value, the stable eigenvalues are located in the triangle in the $\tilde{\sigma_{e1}},\tilde{\sigma_{e2}}$ plane encircled by the straight lines L_{e1},L_{e2},L_{e3}.

Chaos is stabilized at the point where the system's (7) unstable trajectories through a technique known as state feedback control. By introducing a feedback control law as the control force u_{ee}, and using the following formula, the system (7) may be made to take on a controlled form.

$$\begin{aligned} x_{n+1} &= x_n+\frac{\rho^\alpha}{\Gamma(\alpha+1)}\left(rx_n\ln\frac{k}{x_n}-(1-e^{-ax_n})y_n\right)+u_{ee}\\ y_{n+1} &= y_n+\frac{\rho^\alpha}{\Gamma(\alpha+1)}\left((1-e^{-ax_n})y_n-dy_n\right)\\ u_{ee} &= -k_1(x_n-x^+)-k_2(y_n-y^+) \end{aligned} \tag{30}$$

where the nonnegative equilibrium point of the system (7) is represented by (x^+,y^+). The feedback gains are represented by the numbers k_1 and k_2.

Example: To implement the feedback control OGY mechanism for the system (7), we utilize $(a_0,r,k,d,\alpha,\rho)=(1.33,1.2,1.5,0.4,0.75,2.65984)$. In this situation, the unstable system (7) has a single non-negative fixed point $(x^+,y^+)=(0.384079,1.56978)$. Then, based on these parametric values, we offer the controlled system below.

$$\begin{aligned} x_{n+1} &= x_n+2.2662\left(1.2x_n\ln\frac{1.5}{x_n}-(1-e^{-(1.33-\tilde{\sigma_{e1}}(x_n-0.384079)-\tilde{\sigma_{e2}}(y_n-1.56978))x_n})y_n\right),\\ y_{n+1} &= y_n+2.2662\left((1-e^{-(1.33-\tilde{\sigma_{e1}}(x_n-0.384079)-\tilde{\sigma_{e2}}(y_n-1.56978))x_n})y_n-0.4y_n\right). \end{aligned} \tag{31}$$

where the gain matrix is $\tilde{K}=[\tilde{\sigma_{e1}}\quad\tilde{\sigma_{e2}}]$. We also get,

$$\tilde{A_{ee}}=\begin{bmatrix} -0.85338 & -0.90648 \\ 2.83883 & 1 \end{bmatrix}$$

$$\tilde{B_{ee}}=\begin{bmatrix} -0.819801 \\ 0.819801 \end{bmatrix}$$

$$\tilde{C_{ee}}=\begin{bmatrix} -0.819801 & -0.0435314 \\ 0.819801 & -1.50747 \end{bmatrix}$$

Consequently, it is easy to confirm that the matrix's $\tilde{C_{ee}}$ rank is 2. As a result, it is possible to control the system (31), and the Jacobian matrix of its controlled system is given by.

$$\tilde{A_{ee}}-\tilde{B_{ee}}\tilde{K_{ee}}=\begin{bmatrix} -0.85338+0.819801\tilde{\sigma_{e1}} & -0.90648+0.819801\tilde{\sigma_{e2}} \\ 2.83883-0.819801\tilde{\sigma_{e1}} & 1-0.819801\tilde{\sigma_{e2}} \end{bmatrix}$$

The lines L_{e1}, L_{e2} and L_{e3} are offered by for marginal stability.

$$\begin{aligned} L_{e1} &= 0.719959+0.0766677\tilde{\sigma_{e1}}-1.62767\tilde{\sigma_{e2}}=0\\ L_{e2} &= 2.86658+0.896468\tilde{\sigma_{e1}}-2.44747\tilde{\sigma_{e2}}=0\\ L_{e3} &= -2.57334+0.743133\tilde{\sigma_{e1}}+0.807869\tilde{\sigma_{e2}}=0 \end{aligned}$$

The controlled system(31)'s stable triangular region is defined by the marginal lines L_{e1}, L_{e2} and L_{e3}, which are shown in Figure 11.

To investigate the operation of the applied feedback control influence as a controller of chaos in an unstable condition, we performed numerical simulations (see Figure 11). The parameter values will be the same as the OGY method that we select. The chosen feedback increases are $k_1=-0.3$ and $k_2=-0.25$.

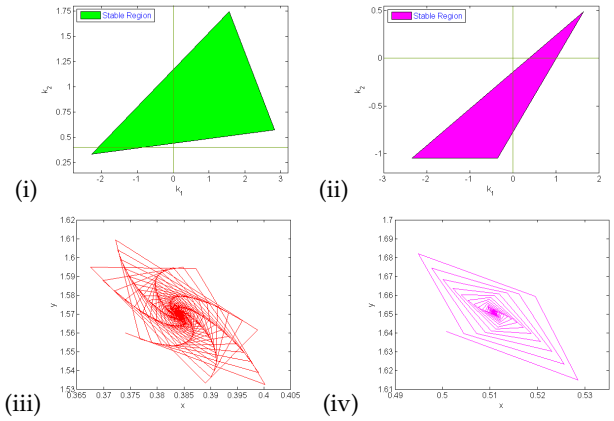

Figure 11 (i-ii) OGY method and State feedback method's stable region (iii-iv) Trajectories of a stable system

CONCLUSION

The present study investigates the dynamics of a model system and identifies two equilibrium points under specific parametric conditions. Our work provides a comprehensive stability analysis of these equilibrium points, which is presented in detail in the paper. In addition, we demonstrate the occurrence of a flip bifurcation and a Neimark-Sacker bifurcation in the model system, both analytically and numerically, under certain conditions. Notably, our results indicate that increasing values of the parameters ρ and a destabilize the system, resulting in a transition from a stable state to chaotic behavior via bifurcation. We observe the resulting chaotic behavior in the models. However, we also demonstrate that the OGY technique can be used to control the chaotic behavior, both numerically and analytically.

Furthermore, our main finding is that the degree of memory represented by the parameter α plays a crucial role in determining the system's behavior. Specifically, our results indicate that strong memory, corresponding to α approaching zero, stabilizes the system, while weak memory, corresponding to α approaching one, leads to chaotic behavior. These findings highlight the importance of memory in the dynamics of the model system.

In summary, this study presents a comprehensive analysis of the dynamics of a model system and demonstrates the occurrence of bifurcations and chaos under specific parametric conditions. Additionally, we show the effectiveness of the OGY technique in controlling the chaotic behavior and highlight the impact of memory on the system's behavior. Our work contributes to a better understanding of the dynamics of the model system and provides insights into the role of memory in the system's behavior.

Availability of data and material

Not applicable.

Conflicts of interest

The authors declare that there is no conflict of interest regarding the publication of this paper.

Ethical standard

The authors have no relevant financial or non-financial interests to disclose.

LITERATURE CITED

Abdelaziz, M., A. Ismail, F. Abdullah, and M. Mohd, 2018 Bifurcations and chaos in a discrete si epidemic model with fractional order. Advances in Difference Equations pp. 1–19.

Abdeljawad, T., 2011 On riemann and caputo fractional differences. Computers & Mathematics with Applications **62**: 1602–1611.

Ahmad, W. and J. Sprott, 2003 Chaos in fractional-order autonomous nonlinear systems. Chaos, Solitons & Fractals **16**: 339–351.

Atabaigi, A., 2020 Multiple bifurcations and dynamics of a discrete time predator-prey system with group defense and non-monotonic functional response. Differential Equations and Dynamical Systems **28**: 107–132.

Berardo, C. and S. Geritz, 2021 Coevolution of the reckless prey and the patient predator. Journal of Theoretical Biology **530**: 110873.

Cartwright, J., 1999 Nonlinear stiffness, lyapunov exponents, and attractor dimension. Physics Letters A **264**: 298–302.

Čermák, J., I. Győri, and L. Nechvátal, 2015 On explicit stability conditions for a linear fractional difference system. Fractional Calculus and Applied Analysis **18**: 651–672.

Cheng, K., S. Hsu, and S. Lin, 1982 Some results on global stability of a predator-prey system. Journal of Mathematical Biology **12**: 115–126.

Connolly, J. A., 2004 The numerical solution of fractional and distributed order differential equations .

Din, Q., 2017 Neimark-sacker bifurcation and chaos control in hassell-varley model. Journal of Difference Equations and Applications **23**: 741–762.

Dzieliński, A., D. Sierociuk, and G. Sarwas, 2010 Some applications of fractional order calculus. Bulletin of the Polish Academy of Sciences: Technical Sciences **4**.

Edward, O., G. Celso, and A. James, 1990 Controlling chaos. Physical Review Letters **64**: 1196–1199.

Elsadany, A. and A. Matouk, 2015 Dynamical behaviors of fractional-order lotka–volterra predator–prey model and its discretization. Journal of Applied Mathematics and Computing **49**: 269–283.

Gompertz, B., 1825 On the nature of the function expressive of the law of human mortality, and on a new mode of determining the value of life contingencies. in a letter to francis baily, esq. frs &c. Philosophical transactions of the Royal Society of London **115**: 513–583.

Guo, G., B. Li, and X. Lin, 2013 Qualitative analysis on a predator-prey model with ivlev functional response. Advances in Difference Equations .

Holling, C., 1965 The functional response of predators to prey density and its role in mimicry and population regulation. The Memoirs of the Entomological Society of Canada **97**: 5–60.

Huang, C., J. Cao, M. Xiao, A. Alsaedi, and F. Alsaadi, 2017a Controlling bifurcation in a delayed fractional predator–prey system with incommensurate orders. Applied Mathematics and Computation **293**: 293–310.

Huang, C., J. Cao, M. Xiao, A. Alsaedi, and T. Hayat, 2018 Effects of time delays on stability and hopf bifurcation in a fractional ring-structured network with arbitrary neurons. Communications in Nonlinear Science and Numerical Simulation **57**: 1–13.

Huang, C., Y. Meng, J. Cao, A. Alsaedi, and F. Alsaadi, 2017b New bifurcation results for fractional bam neural network with leakage delay. Chaos, Solitons & Fractals **100**: 31–44.

Ichise, M., Y. Nagayanagi, and T. Kojima, 1971 An analog simulation of non-integer order transfer functions for analysis of electrode processes. Journal of Electroanalytical Chemistry and

Interfacial Electrochemistry **33**: 253–265.
Işık, S., 2019 A study of stability and bifurcation analysis in discrete-time predator–prey system involving the allee effect. International Journal of Biomathematics **12**: 1950011.
Ivlev, V., 1961 *Experimental ecology of the feeding of fishes*. Yale Univ.
Kangalgil, F. and S. Işık, 2022 Effect of immigration in a predator-prey system: Stability, bifurcation and chaos. AIMS Mathematics **7**: 14354–14375.
Kartal, S., 2014 Mathematical modeling and analysis of tumor-immune system interaction by using lotka-volterra predator-prey like model with piecewise constant arguments. Periodicals of Engineering and Natural Sciences (PEN) **2**.
Kartal, S., 2017 Flip and neimark–sacker bifurcation in a differential equation with piecewise constant arguments model. Journal of Difference Equations and Applications **23**: 763–778.
Khan, A., S. Bukhari, and M. Almatrafi, 2022 Global dynamics, neimark-sacker bifurcation and hybrid control in a leslie's prey-predator model. Alexandria Engineering Journal **61**: 11391–11404.
Kilbas, A., O. Marichev, and S. Samko, 1993 *Fractional integrals and derivatives (theory and applications)*.
Kooij, R. and A. Zegeling, 1996 A predator–prey model with ivlev's functional response. Journal of Mathematical Analysis and Applications **198**: 473–489.
Li, J., G. Sun, and Z. Guo, 2022a Bifurcation analysis of an extended klausmeier–gray–scott model with infiltration delay. Studies in Applied Mathematics **148**: 1519–1542.
Li, J., G. Sun, and Z. Jin, 2022b Interactions of time delay and spatial diffusion induce the periodic oscillation of the vegetation system. Discrete and Continuous Dynamical Systems-B **27**: 2147–2172.
Lynch, S., 2007 *Dynamical systems with applications using Mathematica*. Springer.
M., R., M. D.O., I. P., and J. T., 2011 On the fractional signals and systems. Signal Processing **91**: 350–371.
Marotto, F., 1978 Snap-back repeller imply chaos in rn. J. Math. Anal. Appl. **63**: 199–223.
Marotto, F., 2005 On redefining a snap-back repeller. Chaos, Solit. Fract. **25**: 25–28.
Podlubny, I., 1999 *Fractional Differential Equations*. New York: Academic Press.
Preedy, K., P. Schofield, M. Chaplain, and S. Hubbard, 2007 Disease induced dynamics in host–parasitoid systems: chaos and coexistence. Journal of the Royal Society Interface **4**: 463–471.
Rana, S., 2019 Dynamics and chaos control in a discrete-time ratio-dependent holling-tanner model. Journal of the Egyptian Mathematical Society **27**: 1–16.
Rana, S. and U. Kulsum, 2017 Bifurcation analysis and chaos control in a discrete-time predator-prey system of leslie type with simplified holling type iv functional response. Discrete Dynamics in Nature and Society .
Revilla, T. and V. Křivan, 2022 Prey–predator dynamics with adaptive protection mutualism. Applied Mathematics and Computation **433**: 127368.
Rosenzweig, M., 1971 Paradox of enrichment: Destabilization of exploitation ecosystems in ecological time. Science **171**: 385–387.
Sun, G., H. Zhang, Y. Song, L. Li, and Z. Jin, 2022 Dynamic analysis of a plant-water model with spatial diffusion. Journal of Differential Equations **329**: 395–430.
Uddin, M., S. Rana, S. Işık, and F. Kangalgil, 2023 On the qualitative study of a discrete fractional order prey–predator model with the effects of harvesting on predator population. Chaos, Solitons & Fractals **175**: 113932.
Uriu, K. and Y. Iwasa, 2007 Turing pattern formation with two kinds of cells and a diffusive chemical. Bulletin of mathematical biology **69**: 2515–2536.
Wang, W., L. Zhang, H. Wang, and Z. Li, 2010 Pattern formation of a predator–prey system with ivlev-type functional response. Ecological Modelling **221**: 131–140.
Wei, W., W. Xu, J. Liu, Y. Song, and S. Zhang, 2023 Stochastic bifurcation and break-out of dynamic balance of predator-prey system with markov switching. Applied Mathematical Modelling .
Zhao, M. and Y. Du, 2016 Stability of a discrete-time predator-prey system with allee effect. Nonlinear Analysis and Differential Equations **4**: 225–233.

How to cite this article: Uddin, M. J., Santra, P. K., Rana, S. S., and Mahapatra, G. S. Chaotic Dynamics of the Fractional Order Predator-Prey Model Incorporating Gompertz Growth on Prey with Ivlev Functional Response. *Chaos Theory and Applications*, 6(3), 192-204, 2024.